

SYNTHESIS AND PROPERTIES OF INORGANIC COMPOUNDS

Thin Films of ZnO:M Synthesized by Ultrasonic Spray Pyrolysis

L. N. Demyanets[†], V. V. Kireev, L. E. Li, and V. V. Artemov

Shubnikov Institute of Crystallography, Russian Academy of Sciences, Leninskii pr. 59, Moscow, 117333 Russia

Received May 26, 2010

Abstract—High optical quality ZnO:M@Si nanocomposites (where M is the doping element) were obtained by ultrasonic spray pyrolysis. The variation of experimental conditions, the use of various precursors and dopants demonstrated that the morphology of zinc oxide nanoparticles is mainly determined by the sort of the doping element. The luminescence spectra confirm indirectly the isomorphous incorporation of the dopant ions into the zinc oxide lattice.

DOI: 10.1134/S0036023611100056

Zinc oxide is a well-known wide bandgap semiconductor having a unique set of physical properties, which determine its practical value for many fields of technology. Particular attention is attracted by nanocrystalline zinc oxide as a material of modern nanotechnology in the fields of photonics, spintronics, laser physics, and others [1–4]. The scope of applications of small-sized ZnO is markedly extended by using iso- or heteroisomorphous substitution in the oxide structure. The M⁺ (Li, H), M²⁺ (Be, Mg, Fe, Co, Ni, Mn, etc.), M³⁺ (In, Ga, Cr, Ln, Al, etc.), M⁵⁺ (Sb, P, N, V), and M⁶⁺ ions (S) ions have been admixed to zinc oxide [5–18]. The incorporation of dopant ions into the lattice changes the band gap width, gives rise to new physical characteristics (magnetic, piezoelectric, optical, spectroscopic, and chemical characteristics). The dopants function as either donors or acceptors. The key substitution dopants that function as donors include the Group III elements M³⁺, which occupy cationic sites, Group VII elements (F, Cl), which occupy anionic sites of the crystal lattice, and M⁺ (Li, H). The introduction of these ions into the zinc oxide lattice increases the electrical conductivity. For the formation of acceptors in the compounds A^{II}B^{VI}, it is necessary to replace a Group II element by a Group I cation and to replace a Group VI element by a Group V anion. Such a doping suppresses the *n*-type conductivity; this is actually observed upon doping of zinc oxide with Sb, P, N giving rise to *p*-type conductivity.

Nanocrystalline ZnO doped with various elements is prepared using the same set of methods as are used to obtain a nominally pure material, in particular, crystallization methods from the liquid, gas, or solid phase [3, 19–25].

The purpose of this work was to obtain In-, Ga-, and P-doped ZnO nanocrystals and films in order to elucidate the effect of dopants on the morphology and physical properties of ZnO:M.

[†] Deceased.

EXPERIMENTAL

Synthesis. ZnO films were prepared by crystallization of ZnO upon thermal decomposition of the aerosol obtained by ultrasonic dispersion of a precursor solution (ultrasonic spray pyrolysis, USP).

The ultrasonic aerosol generator produces an aerosol consisting of ultradisperse drops of several micrometer size above the solution surface. Fast heating of the drops induces evaporation of the solvent, heating and decomposition of the precursor, and chemical reaction between the starting compounds (Fig. 1). It is very important that in this case, homogenization occurs at the molecular level, because a true solution is atomized. Thus, using precursors of a complex composition, it is possible to obtain doped particles.

An experimental setup was designed for sputtering of zinc oxide crystallites. The schematic view of the setup is presented in Fig. 2. A Liiot humidifier (Korea) was used as the ultrasonic aerosol generator. The sputtering chamber was a 1.5 m-long quartz tube heated with a tube furnace at the bottom. Owing to the sufficient height of the tube and high temperature in the sputtering chamber, a convective flow is formed, which ensures the vertical migration of the aerosol mixture. The substrates are placed in the tube on a heat-resistant alloy wire. This setup allows one to perform deposition on numerous substrates in one experiment; for each substrate, the path lengths of the aerosol drops and nascent particles (the distance from the generator nozzle to the substrate, *L*) and temperature are known. Since the temperature is changed along the height of the sputtering chamber, the dependence of the substrate temperature on the substrate position in the chamber (and, hence, on *L*) was studied at different rated temperatures measured by the control thermocouple. The results of this study for some *T_c* values are presented in Fig. 3. Using this plot, it is possible to estimate the real temperature of each substrate in the experiment.

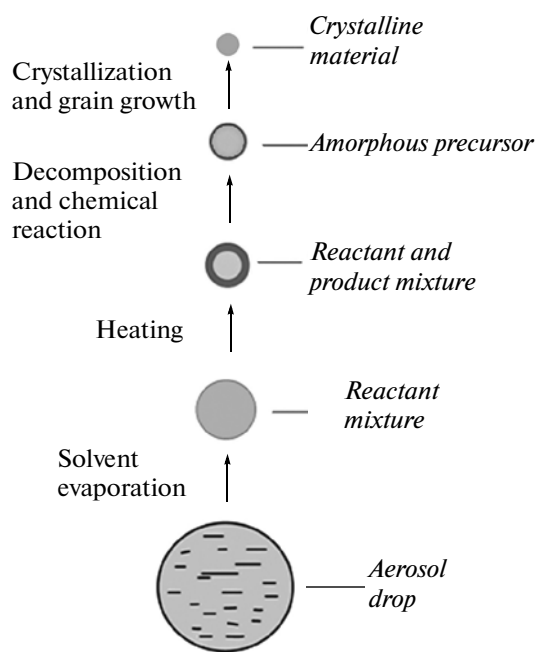


Fig. 1. Scheme of crystallite formation by USP.

Experimental conditions. The experiments were carried out with the following variable parameters: zinc acetate, formate, or nitrate as the precursor; precursor concentration, 0.02–0.05 mol/L; Si(111), Si(100) as the substrate; T_c (measured by the control thermocouple), 550–770°C; substrate temperature T (determined from the plot in Fig. 3), 200–665°C; sputtering time, 8–28 h; nozzle–substrate distance $L = 7$ –35 cm; doping additives, Ga, In, P, Li. The atomic ratio of zinc to the doping element Zn : M was 25 : 1 to 50 : 1.

A solution of zinc acetate was prepared by dissolving $\text{Zn}(\text{CH}_3\text{COO})_2 \cdot 2\text{H}_2\text{O}$ in distilled water and addition of acetic acid (5 to 10 drops per liter) to avoid hydrolysis. A solution of zinc nitrate was prepared by dissolving $\text{Zn}(\text{NO}_3)_2 \cdot 6\text{H}_2\text{O}$ in distilled water. A solution of zinc formate was prepared by dissolving zinc oxide in formic acid.

Zinc oxide was doped by indium or gallium by dissolving $\text{Ga}(\text{CH}_3\text{COO})_2\text{OH}$ or presynthesized $\text{In}(\text{OH})_3$ in a small amount of acetic or formic acid. For phosphorus or phosphorus–lithium doping, solutions of ammonium dihydrogen phosphate ($\text{NH}_4\text{H}_2\text{PO}_4$) or lithium dihydrogen phosphate (LiH_2PO_4) were prepared. An appropriate amount of the solution containing a doping element was added to the zinc-containing solution.

Characterization of products. The obtained products were characterized by the following procedures:

— powder X-ray diffraction (XRD-6000 Shimadzu diffractometer, $\text{CuK}\alpha$ radiation);

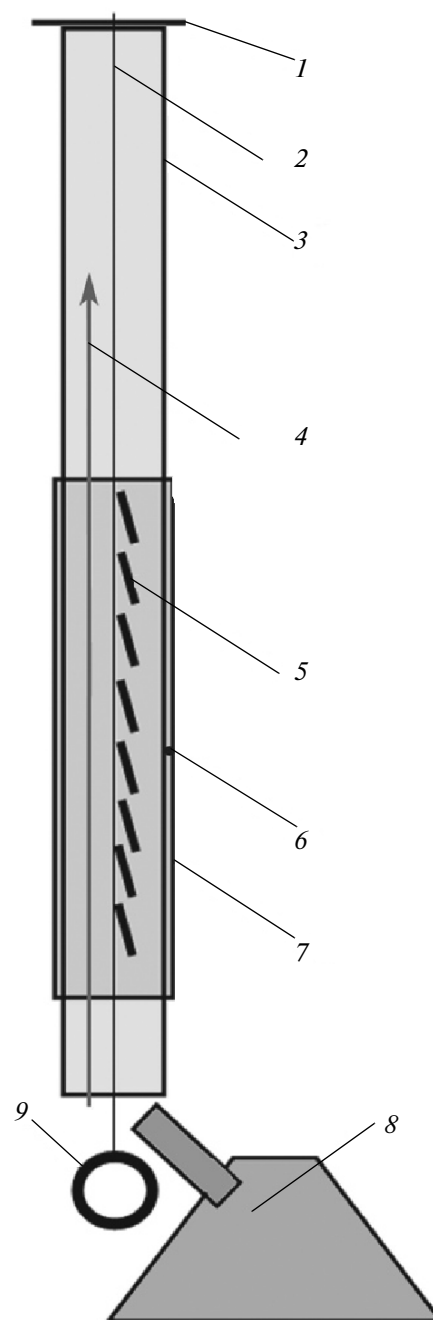


Fig. 2. Schematic diagram of the USP sputtering setup with convective transfer of aerosol. (1) carrier arm for the wire, (2) refractory wire, (3) quartz tube, (4) direction of the aerosol migration, (5) substrates, (6) control thermocouple, (7) furnace, (8) ultrasonic aerosol generator, (9) load.

— scanning electron microscopy (JEOL JSM-7401F);

— optical spectroscopy.

RESULTS AND DISCUSSION

A series of ZnO:M@Si(111) nanocomposites was prepared as crystallites of zinc oxide activated by dopant ions and supported on the substrate. The character of the coating formed on the substrates by sputtering is substantially affected by the sample position in the furnace (sputtering chamber). This is related to specific features of particle formation by the USP (Fig. 1). In the lower part of the sputtering chamber, the solvent (water) has not been entirely removed and the particles are deposited on the substrate as a solution, and crystallization takes place on the surface and does not differ from usual crystallization taking place on evaporation. No nanoparticle film is formed in this way. In the middle part of the sputtering chamber, both the temperature and the residence time of a particle in the hot area are greater, the solvent has been removed, and the particles are at the stage of formation and have not yet completely crystallized. The particles have an active surface and interact with one another to give a dense film, which usually looks like a tarnish. The upper part of the sputtering chamber contains many particles whose residence time in the furnace is sufficient for the formation of well-crystallized particles with a passive surface. On deposition on the substrate, they do not form a thin film but form a white bloom (or yellowish one in the case of indium doping). This bloom has low adhesion to the substrate and can be readily manually removed, whereas the film formed in the middle area is rather dense and cannot be manually removed.

The composition of the obtained films was determined directly by energy-dispersive analysis (EDA) and indirectly based on variation of the emission spectra as compared with the spectra of nominally pure zinc oxide, indicating incorporation of the dopant. The fact that the obtained films correspond to the hexagonal ZnO modification, wurtzite structural type, was confirmed by powder X-ray diffraction and EDA (Fig. 4).

The morphology of the crystallites constituting the film (pyramidal, bipyramidal, prismatic, elongated, and platy ones) is governed by the experimental parameters. The typical morphology of the ZnO:M crystallites is shown in Figs. 5–7. The main crystallographic simple forms forming the faceting are monohedron {0001}, pyramid {10 $\bar{1}$ 1}, and prism {10 $\bar{1}$ 0}.

Figure 5 shows the typical morphology of indium-activated ZnO crystallites obtained using aqueous solutions of zinc acetate and formate as the precursors. On attempted synthesis of similar crystallites from nitrate precursors, the solution grew turbid during the experiments and, hence, the solution composition changed and the crystal formation pattern could not be properly interpreted. At temperatures of ~200°C, dispersion of acetate solutions afforded substrate-deposited aggregates composed of ZnO particles with an average size of ~200 nm. The particles had a tabular habit with feebly developed pyramid faces (Fig. 5a). As

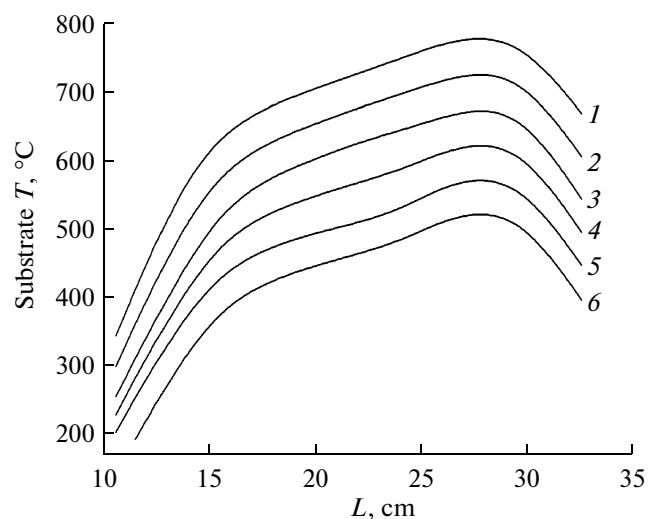


Fig. 3. Substrate temperature T in the sputtering chamber vs. distance from the substrate to the ultrasonic generator nozzle (L) at the nominal temperature of the experiment T_c : (1) 800, (2) 750, (3) 700, (4) 650, (5) 600, (6) 550°C.

the substrate temperature was raised to 450°C, the particle morphology was retained; however, pyramid {000 $\bar{1}$ } became the most developed simple form along with monohedron (10 $\bar{1}$ 1); the c axis was perpendicular or inclined to the substrate surface (Fig. 5b), no particle aggregation took place. On further increase in the substrate temperature to 580°C, the pyramid faces disappeared, 250–500 nm regular (0001) aggregates of plate crystals are formed (Fig. 5c). Crystallization of zinc formate solutions gives rise to a film of 200–300 nm close-packed plate crystals and several μ m large aggregates of plate crystals (Fig. 5d).

The introduction of gallium compounds to the growth system results in the formation of crystallites mainly shaped as truncated pyramids (Fig. 6). The most clear-cut pyramidal faceting is observed when nitrate precursors are used (Figs. 6a, 6b). The particle size is 100–300 nm, and the (0001) surface is composed of numerous layers with thickness of up to 10 nm, which is indicative of two-dimensional nucleation on these surfaces. As the temperature is raised from 440 to 510°C, the monohedron (0001) faces almost disappear (the growth rate along the [0001] direction increases), and simple pyramid shape {10 $\bar{1}$ 1} develops. At 510°C, a film composed of close-packed zinc oxide particles shaped like hexagonal pyramids is obtained, the c axis being perpendicular to the substrate surface (Fig. 6b). When gallium-doped zinc oxide is synthesized from formate and acetate solutions, the characteristic particle size is 1 μ m, which is several times larger than that formed with nitrate precursors (Figs. 6c–6f). The pyramidal faceting of the particles obtained from formate solutions at 560°C was not very clearly defined and, hence, the particles looked rounded (Fig. 6c). As the temperature was raised to 655°C, the pyramidal

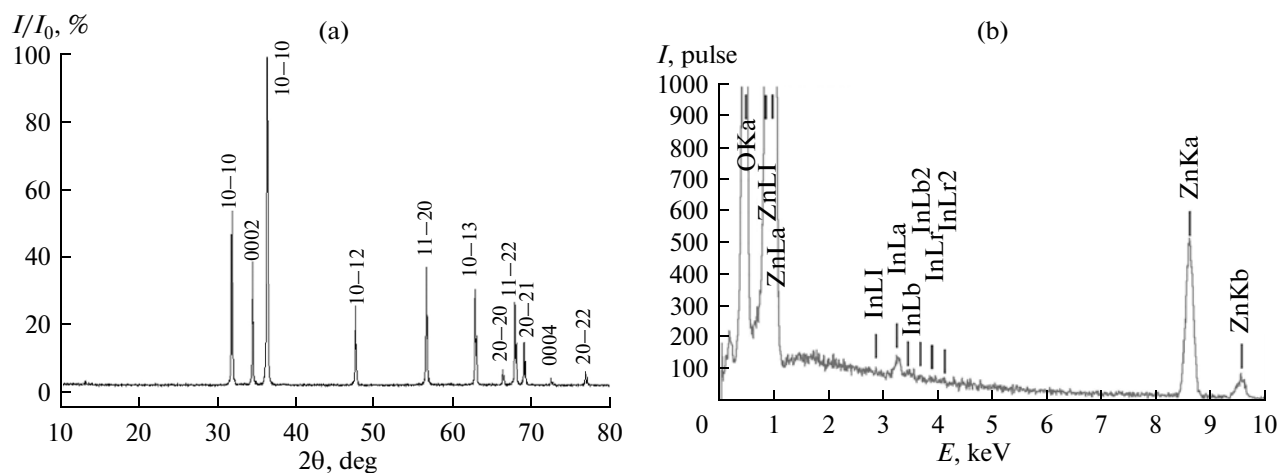


Fig. 4. Data of (a) energy dispersive analysis and (b) powder X-ray diffraction analysis.

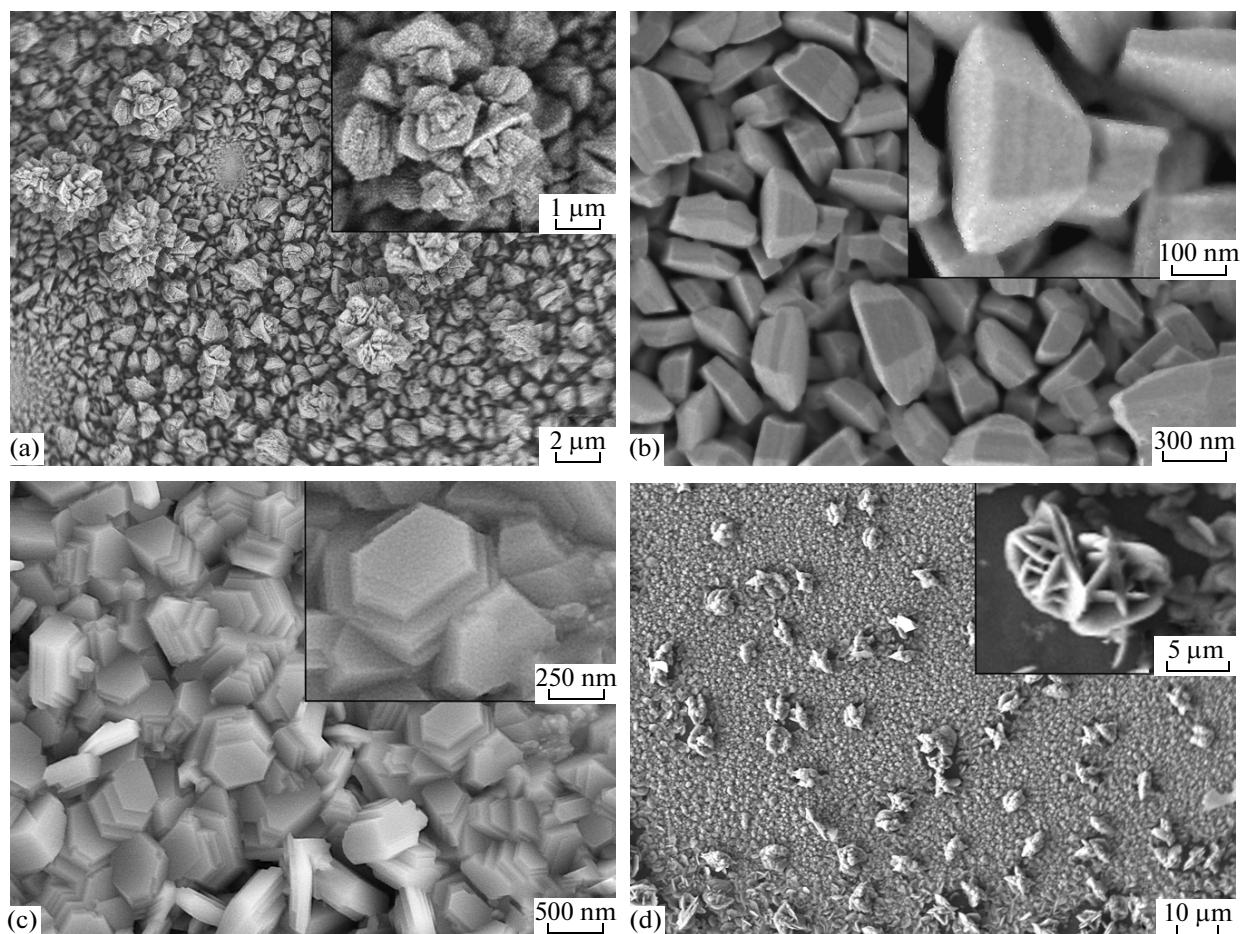


Fig. 5. Photomicrographs of ZnO:In samples synthesized under different conditions. (a) $\text{Zn}(\text{CH}_3\text{COO})_2$ as the precursor; concentration $c = 0.02$ mol/L; atomic ratio $R_{\text{at}} = \text{Zn} : \text{In} = 50 : 1$, $T = 200^\circ\text{C}$; (b) $\text{Zn}(\text{CH}_3\text{COO})_2$ as the precursor, $c = 0.02$ mol/L, $R_{\text{at}} = 50 : 1$, $T = 450^\circ\text{C}$; (c) $\text{Zn}(\text{CH}_3\text{COO})_2$ as the precursor, $c = 0.02$ mol/L, $R_{\text{at}} = 25 : 1$, $T = 580^\circ\text{C}$; (d) $\text{Zn}(\text{HCOO})_2$ as the precursor, $c = 0.05$ mol/L, $R_{\text{at}} = 25 : 1$, $T = 565^\circ\text{C}$.

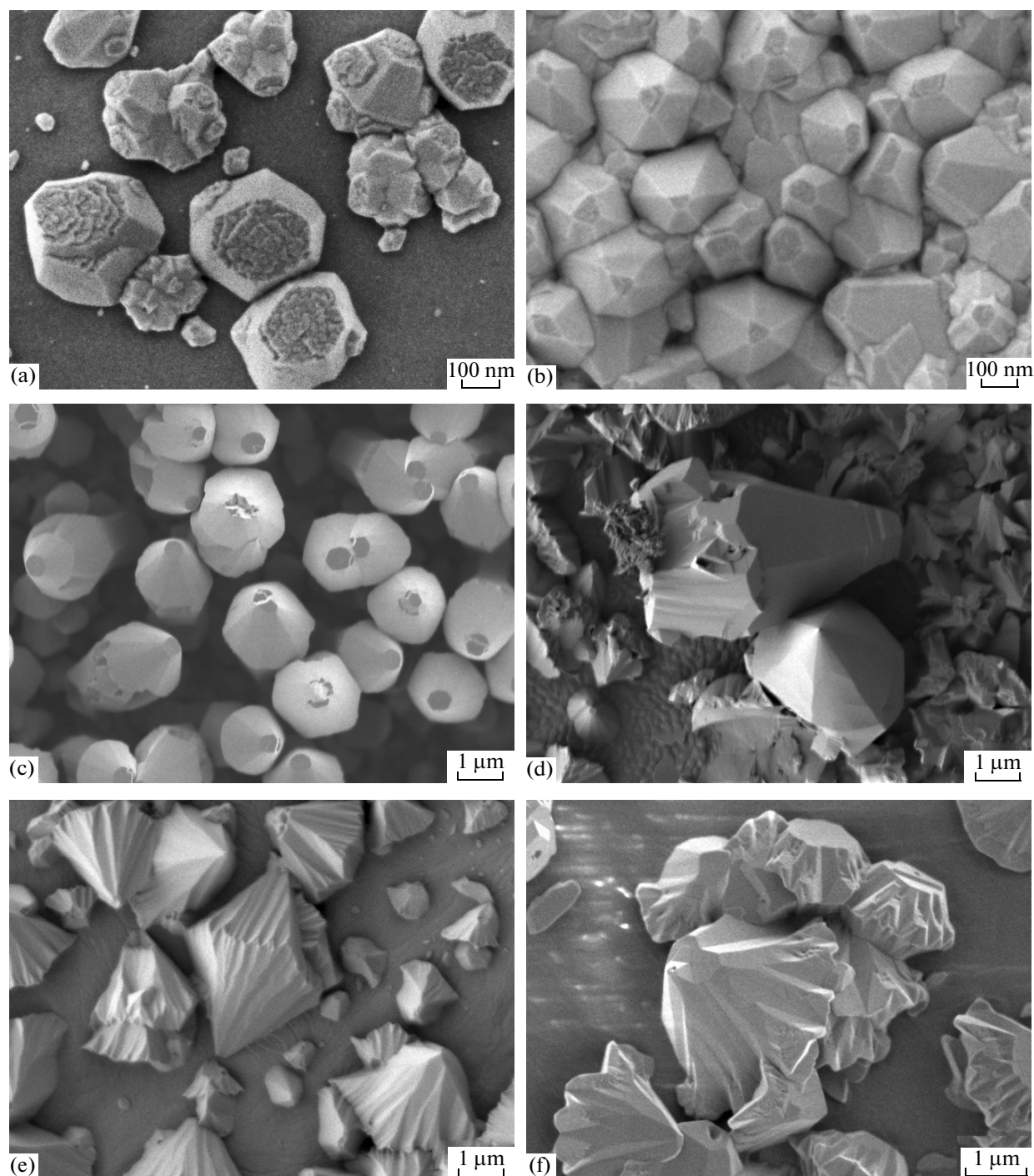


Fig. 6. Photomicrographs of ZnO:Ga samples synthesized under different conditions. (a) $\text{Zn}(\text{NO}_3)_2$ as the precursor, $c = 0.02$ mol/L, atomic ratio $R_{\text{at}} = \text{Zn} : \text{Ga} = 50 : 1$, $T = 440^\circ\text{C}$; (b) $\text{Zn}(\text{NO}_3)_2$ as the precursor, $c = 0.02$ mol/L, $R_{\text{at}} = 50 : 1$, $T = 510^\circ\text{C}$; (c) $\text{Zn}(\text{HCOO})_2$ as the precursor, $c = 0.02$ mol/L, $R_{\text{at}} = 50 : 1$, $T = 560^\circ\text{C}$; (d) $\text{Zn}(\text{HCOO})_2$ as the precursor, $c = 0.02$ mol/L, $R_{\text{at}} = 25 : 1$, $T = 655^\circ\text{C}$; (e) $\text{Zn}(\text{CH}_3\text{COO})_2$ as the precursor, $c = 0.02$ mol/L, $R_{\text{at}} = 25 : 1$, $T = 515^\circ\text{C}$; (f) $\text{Zn}(\text{CH}_3\text{COO})_2$ as the precursor, $c = 0.02$ mol/L, $R_{\text{at}} = 25 : 1$, $T = 640^\circ\text{C}$.

faceting was clearly defined (Fig. 6d); however, in this case, apart from large ($>1 \mu\text{m}$) particles, numerous particles with sizes of hundreds nanometers were present on the substrate. The particles synthesized from acetate solutions have a specific feature not

observed in other cases, in particular, the pyramid faces are complicated by additional faceting to form a cone with a corrugated surface (Figs. 6e, 6f).

Using phosphorus (and phosphorus together with lithium) as the doping element, samples obtained

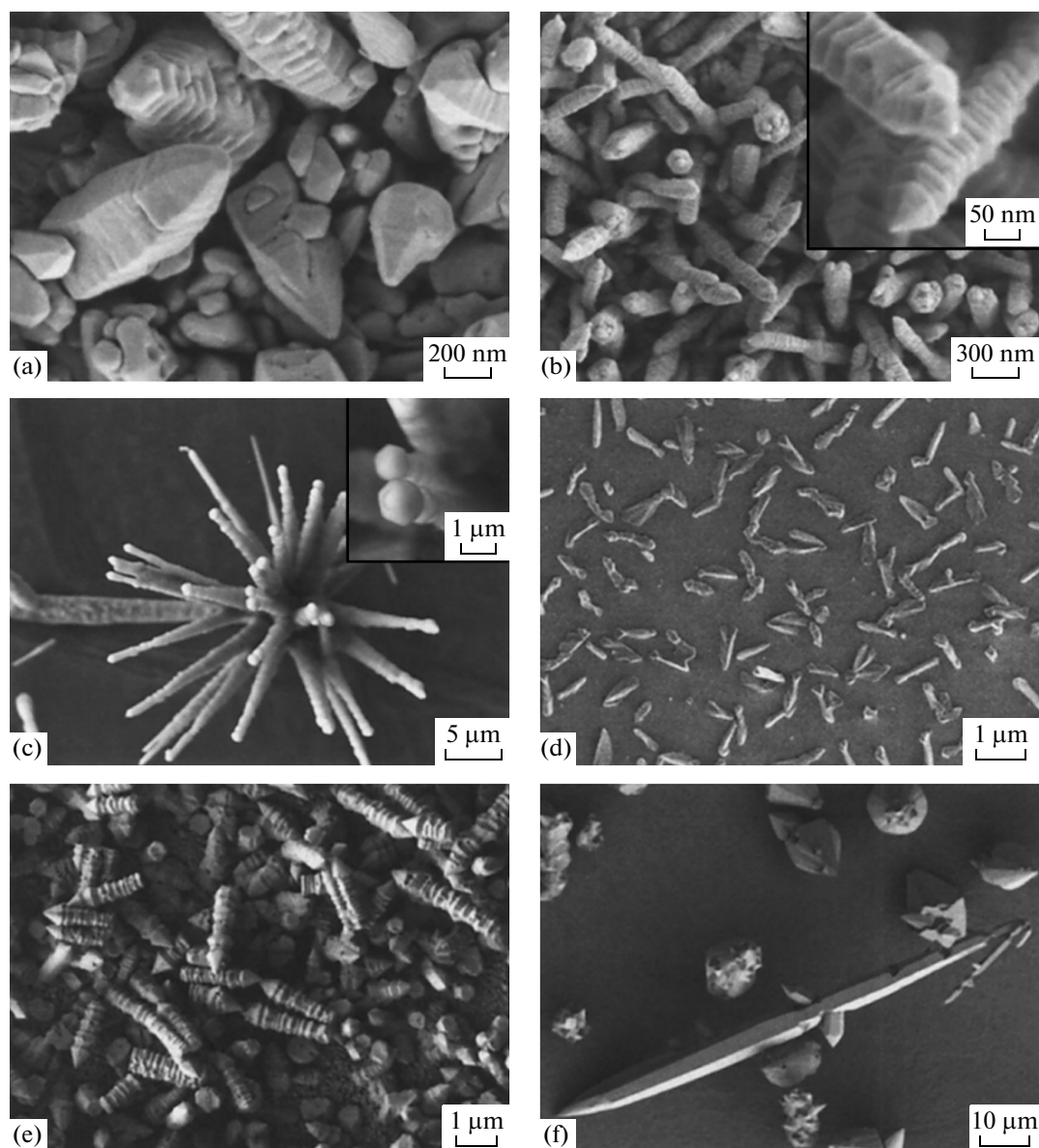


Fig. 7. Photomicrographs of ZnO:P samples synthesized under different conditions; atomic ratio $R_{\text{at}} = \text{Zn} : \text{P} = 50 : 1$. (a) $\text{Zn}(\text{CH}_3\text{COO})_2$ as the precursor, concentration $c = 0.02$ mol/L, $T = 520^\circ\text{C}$; (b) $\text{Zn}(\text{CH}_3\text{COO})_2$ as the precursor, $c = 0.02$ mol/L, $T = 520^\circ\text{C}$, sapphire as the substrate; (c) $\text{Zn}(\text{HCOO})_2$ as the precursor, $c = 0.05$ mol/L, $T = 575^\circ\text{C}$; (d) $\text{Zn}(\text{HCOO})_2$ as the precursor, $c = 0.02$ mol/L, $T = 515^\circ\text{C}$; (e) $\text{Zn}(\text{HCOO})_2$ as the precursor, $c = 0.02$ mol/L, $T = 600^\circ\text{C}$; (f) $\text{Zn}(\text{HCOO})_2$ as the precursor, $c = 0.02$ mol/L, $T = 640^\circ\text{C}$.

from acetate and formate solutions were synthesized and studied. On attempted preparation of nitrate precursors, a precipitate separated from the solution; therefore, sputtering was not performed in this case. Phosphorus doping was found to give rise to polysynthetic twins with (0001) intergrowth plane; this gives rise to long-prismatic aggregates ending with a pyramid or a positive monohedron (Fig. 7). For the synthesis from acetate solutions, sputtering was carried out not only on silicon (Fig. 7a) but also on sapphire substrates (Fig. 7b). In both cases, crystallites with

similar morphology were formed. The aggregate diameter was ~ 100 nm on sapphire substrates and several hundreds nm on silicon substrates. Particles of the same morphology are formed in the synthesis from the formate precursor and combined lithium and phosphorus doping (Fig. 7c). In this case, the elongated aggregates often grow from the same site, while in the case of phosphorus doping and use of acetate solutions considered previously, the aggregates are arranged randomly on the substrate. Doping with phosphorus and the use of formate solutions at 515°C affords

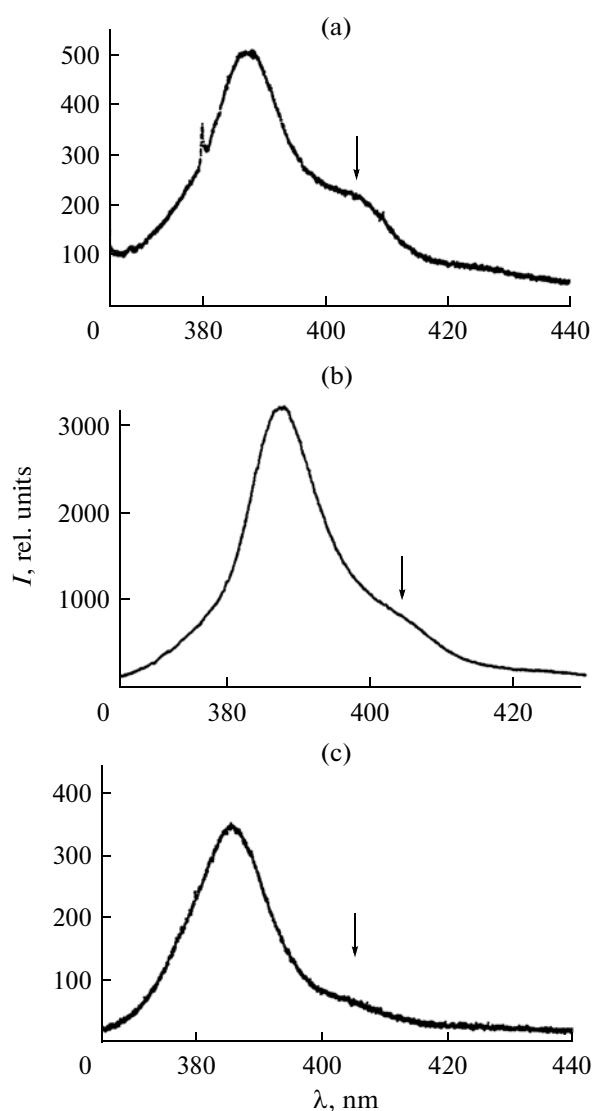


Fig. 8. Luminescence spectra of the ZnO@Si(111) nanocomposites activated by (a) indium, (b) gallium, and (c) phosphorus. The arrows mark the new bands related to the recombination of excitons localized on the dopant centers.

aggregates of elongated prismatic and pyramidal crystals of diameters up to 300 nm and lengths of up to several μm (Fig. 7d). As the temperature is raised to 600–640°C, prismatic crystals confined by pyramids are formed. The crystal diameter is up to 1 μm and the length is about several μm (Figs. 7e, 7f). Apart from these elongated crystals, pyramidal crystals resembling those obtained on gallium doping are also present on the substrate (Fig. 6).

Comparison of the SEM images of the sputtered samples deposited under various conditions indicates that the morphology of doped particles depends most appreciably on the sort of the doping element and depends to a lesser extent on the substrate temperature and on the precursor used (nitrate, acetate, or formate).

Figure 8 shows typical luminescence spectra of the doped nanocomposites ZnO:M. The presence of intense exciton luminescence attests to the high optical quality of the obtained material and to the absence of quenching centers at the dopant concentrations used. The luminescence spectra of activated zinc oxide show a new long-wavelength peak (Fig. 8). This peak is related to recombination of excitons localized on the dopant centers, as noted in a previous publication [26]. The appearance of this band is indirect evidence for the isomorphous incorporation of dopant ions into the zinc oxide lattice.

This is of the greatest interest for the case of zinc oxide activation by phosphorus ions, as the activation with phosphorus forms ZnO material with *p*-type conductivity, which opens up broad prospects for the design of light emitting semiconductor devices based on this composite.

Thus, ZnO:M@Si nanocomposites (M is a doping element, In, Ga, or P) of high optical quality were produced by ultrasonic spray pyrolysis of aqueous solutions of the precursors. The morphology of ZnO crystallites formed on Si(111) and the appearance of the film are determined by the type of the precursor, the presence of doping additives, the substrate temperature, and the distance from the substrate to the ultrasonic generator nozzle. The EDA and luminescence spectral data confirm the incorporation of the dopant ions into the zinc oxide lattice.

REFERENCES

1. Ü. Özgür, Ya. I. Alivov, C. Liu, et al., *J. Appl. Phys.* **98**, 041301 (2005).
2. L. Schmidt-Mende and J. L. MacManus-Driscoll, *Mater. Today* **10** (5), 40 (2007).
3. S. J. Pearton, D. P. Norton, K. Ip, et al., *Prog. Mater. Sci.* **50** (3), 293 (2005).
4. S. J. Pearton, C. R. Abernathy, G. T. Thaler, et al., *Materials Today* **9** (11), 34 (2002).
5. B. Martínez, F. Sandiumenge, Ll. Balcells, et al., *Phys. Rev.* **72**, 165202.
6. A. R. Raju and C. Rout, in *Proceedings of ICMAT 2005 & IUMRS-ICAM 2005, Materials Research Society of Singapore* (Singapore, 2005), p. 13.
7. L. Q. Liu, B. Xiang, X. Z. Zhang, et al., *Appl. Phys. Lett.* **88**, 063104 (2006).
8. J. J. Liu, M. H. Yu, W. L. Zhou, et al., *J. Appl. Phys.* **99**, 08M119 (2006).
9. D. Iusan, R. Knut, B. Sanyal, et al., *Phys. Rev. B: Condens. Matter* **78**, 085319 (2008).
10. C. R. Ding, S. W. Li, and H. Z. Wang, *Appl. Phys. Lett.* **90**, 241918 (2007).
11. A. S. Gonçalves, M. R. Davolos, N. Masaki, et al., *Dalton Trans.*, No. 11, 1487 (2008).
12. H. Wang, H. P. Ho, K. C. Lo, and K. W. Chean, *J. Phys. D: Appl. Phys.* **40** (15), 4682 (2007).
13. L. M. Li, C. C. Li, J. Zhang, et al., *Nanotechnology* **18**, 225504 (2007).

14. Y. Bai, Y. Wang, K. Yang, et al., *J. Phys. Chem.* **112** (32), 12259 (2008).
15. P. Mohanty, B. Kim, and J. Park, *Mat. Sci. Eng: B* **138** (3), 24 (2007).
16. B. Q. Cao, M. Lorenz, A. Rahm, et al., *Nanotechnology* **18** (45), 455707 (2007).
17. J. V. Foreman, J. Li, H. Peng, et al., *Nano Lett.* **6** (6), 1126 (2006).
18. Y. C. Yang, C. Song, X. H. Wang, et al., *Appl. Phys. Lett.* **92**, 012907 (2008).
19. G.-C. Yi, C. Wang, and P. Won II, *Semicond. Sci. Technol.* **20**, 22 (2005).
20. W.-T. Yao and S.-H. Yu, *Int. J. Nanotechnol. (IJNT)* **4** (1–2), 129 (2007).
21. L. Chen, N. Bao, K. Yamagisawa, et al., *Cryst. Growth Des.* **7** (12), 2742 (2007).
22. J. Elias, R. Tena-Zaera, and C. Lévy-Clément, *J. Phys. Chem. C* **112** (15), 5736 (2008).
23. X. Liu, X. Wu, H. Cao, and R. P. H. Chang, *J. Appl. Phys.* **95** (6), 3141 (2004).
24. J.-L. Zhao, X.-M. Li, S. Zhang, et al., *Mater. Today* **21** (9), 2185 (2006).
25. L. N. Dem'yanets, L. E. Li, T. G. Uvarova, and Yu. M. Mininzon, *J. Mater. Sci.* **43**, 2143 (2008).
26. H. Kato, M. Sano, K. Miyamoto, et al., *J. Cryst. Growth* **237–239** (Part 1), 538 (2002).